

# Creation and Control of Vortex-Beam Arrays in Atomic Vapor

Jinpeng Yuan, Hengfei Zhang, Chaohua Wu, Gang Chen,\* Lirong Wang,\* Liantuan Xiao, and Suotang Jia

**Optical vortices, which are beams with spiral-shaped wavefronts and screw phase dislocations, have potential for supporting high-capacity optical communications. In this study, the generation of 1D and 2D vortex-beam arrays is theoretically proposed and experimentally demonstrated by introducing novel forked-photonic lattices in a three-level  $^{85}\text{Rb}$  atomic medium. Such forked-photonic lattices are established through the interference of Gaussian and vortex coupling beams. The input Gaussian probe beam that travels through this lattice experiences phase superposition and is diffracted into vortex-beam arrays. Moreover, the relative efficiency of the high-order diffractions can be enhanced by tuning the two-photon detuning and power of the coupling beams. The enriched diffractive arrays of a vortex probe beam propagating in such forked-photonic lattices are also presented. The experimental results agree well with those of the numerical simulations. This work suggests that atomic systems are a fertile platform for creating and controlling vortex-beam arrays, and that they can shed light on ongoing exploration in the fields of optical manipulation and quantum information processing.**

multiplexing dimension for improving the capacity and security of optical communication systems.<sup>[4,5]</sup> Notably, forked-diffractive elements, such as forked gratings, Dammann gratings, and forked holographic phase patterns, are good candidates for converting a Gaussian beam into a series of vortex beams.<sup>[6–10]</sup> Similar forked-shaped structures can also be implemented in solid materials by femtosecond laser direct writing.<sup>[11,12]</sup> Moreover, forked-related structures in metasurfaces have been widely employed to generate large vortex-beam arrays,<sup>[13–16]</sup> fulfilling the requirement of a large data storage capacity by the parallel processing of vortex beams.<sup>[4,9]</sup> While these devices only realize the photonic design programmed by the manufacturer without exhibiting any further versatility in adherence to diverse designs, losing the appeal of an on-demand system.

## 1. Introduction

With the increasing demand for improved capacity and speed in data transmission, researchers have been seeking new multiplexing dimensions, apart from those for amplitude, frequency, and polarization, to satisfy the requirements of next-generation optical communication. Vortex beams, which possess a null-intensity phase singularity at the beam center and a tunable orbital angular momentum (OAM) mode,<sup>[1–3]</sup> have provided an additional

On the other hand, the photonic lattices assisted by electromagnetically induced transparency (EIT) in multilevel atomic medium are attractive systems for exploring the control of light.<sup>[17]</sup> In such optically-induced lattices, the refractive index of the probe beam is spatially manipulated by a standing-wave field, which is established by the interference of the coupling beams. Accordingly, the atomic system acts as a grating and diffracts the probe beam. Compared to solid-state systems, optical lattices in an atomic medium can be more flexibly tuned and easily reconfigured owing to the various coherent control techniques enabled by EIT,<sup>[18]</sup> resulting in easily controllable absorption, dispersion,<sup>[19,20]</sup> Raman gain,<sup>[21–23]</sup> and nonlinearity.<sup>[24]</sup> Recently, several physical effects have been demonstrated in this system, such as parity-time symmetry,<sup>[22,25]</sup> Talbot effect,<sup>[26,27]</sup> Bloch oscillation and Zener tunneling,<sup>[28]</sup> photonic Floquet topological insulators,<sup>[29]</sup> flat bands,<sup>[30]</sup> and edge states and spin-orbit coupling in photonic graphene.<sup>[31,32]</sup> These studies suggest that the atomic medium can be a promising ground for creating and manipulating vortex-beam arrays that have not been experimentally realized.

In this study, we theoretically propose and experimentally demonstrate the generation of one-dimensional (1D) and two-dimensional (2D) vortex-beam arrays by introducing novel forked-photonic lattices in a three-level  $^{85}\text{Rb}$  atomic medium. Such photonic lattices, which have  $m$  dislocation defects inside the atomic vapor cell, are established by the interference of Gaussian and vortex (with topological charge  $m$ ) coupling beams, and a weak probe Gaussian beam is launched into it. Consequently,

J. Yuan, H. Zhang, C. Wu, G. Chen, L. Wang, L. Xiao, S. Jia  
State Key Laboratory of Quantum Optics and Quantum Optics Devices  
Institute of Laser Spectroscopy  
Shanxi University

92 Wucheng Road, Taiyuan 030006, China  
E-mail: chengang971@zzu.edu.cn; wlr@sxu.edu.cn

J. Yuan, H. Zhang, C. Wu, G. Chen, L. Wang, L. Xiao, S. Jia  
Collaborative Innovation Center of Extreme Optics  
Shanxi University  
92 Wucheng Road, Taiyuan 030006, China

G. Chen  
School of Physics and Microelectronics  
Key Laboratory of Materials Physics of Ministry of Education  
Zhengzhou University  
Zhengzhou 450001, China

 The ORCID identification number(s) for the author(s) of this article can be found under <https://doi.org/10.1002/lpor.202200667>

DOI: 10.1002/lpor.202200667

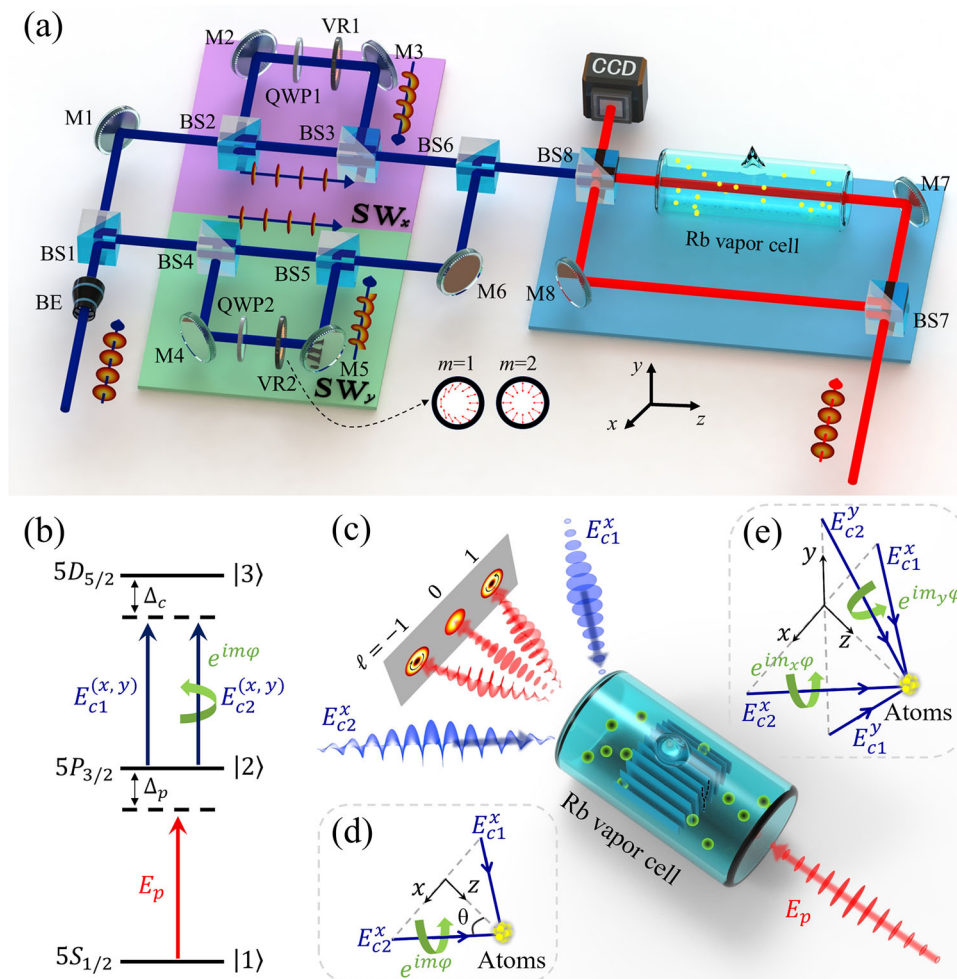


**Figure 1.** a) Experimental setup for generating vortex-beam arrays. BE: beam expander; BS: 50/50 beam splitter; M: high reflection mirror; QWP: quarter-wave plate; VR: vortex retarder; CCD: charge-coupled device. b) Relevant energy levels of the cascade-type three-level configuration in  $^{85}\text{Rb}$  atomic vapor. c) Schematic illustration of generation of 1D vortex-beam arrays. d,e) Geometrical arrangement of the crossed coupling beams for 1D and 2D forked coupling-fields. Spiral phases of the coupling beams for 2D are denoted by  $e^{im_x\varphi}$  and  $e^{im_y\varphi}$ .

a discrete diffraction pattern of the probe field with the topological charges  $\ell$ , that is, vortex-beam arrays, can be obtained at the output plane of the vapor cell. These topological charges depend on the diffraction order  $n$  and topological charge  $m$ . Moreover, the relative efficiency of high-order diffractions can be controlled through system parameters such as two-photon detuning and the power of the coupling beams. Finally, the diffractions of the vortex probe beam experiencing such forked-photonic lattices are demonstrated, which provide flexible tunability of the generated vortex-beam arrays.

Our scheme is novel in the following ways. First, the forked-photonic lattices induced in the atomic ensemble offer easier accessibility and better tunability than solid materials do. Second, our system is scalable, allowing the creation of large square-shaped vortex-beam arrays and the exploration of many other complex geometric configurations of vortex-beam arrays by exploiting the versatility of the design supported by multi-beam interference. Third, the vortex-beam arrays are created and controlled all-optically, enabling this system to be integrated as a novel all-optical device, which can provide tunable degrees of

freedom in fields such as optical manipulation, optical machining, and optical communication.

## 2. Production of Forked-Photonic Lattices in Rb Atomic Vapor

Our experiments (schematically depicted in **Figure 1a**) are carried out in an  $^{85}\text{Rb}$  vapor cell with a cascade-type three-level atomic configuration consisting of  $|1\rangle = |5S_{1/2}\rangle$ ,  $|2\rangle = |5P_{3/2}\rangle$ , and  $|3\rangle = |5D_{5/2}\rangle$  (**Figure 1b**). A Gaussian-shaped coupling beam  $E_c^x$  (with wavelength  $\lambda_c = 776$  nm, frequency  $\omega_c$ ), derived from a tapered-amplified diode laser (TA pro, Toptica), is split into two beams  $E_{c1}^x$  and  $E_{c2}^x$  (with wave vector  $k_{c1}^x$  and  $k_{c2}^x$ , respectively) with similar intensities and spatial shapes using a beam splitter (BS2). One beam (i.e.,  $E_{c2}^x$ ) is converted into a vortex beam with a spiral phase  $e^{im\varphi}$  after passing through a quarter-wave plate (QWP1) and vortex retarder (VR1),<sup>[33]</sup> where  $m$  and  $\varphi$  are the topological charge and azimuthal angle, respectively. To construct a forked coupling-field, these two beams encounter at a beam splitter (BS3) with a small angle  $2\theta \approx 0.6^\circ$  in the  $x$ - $z$  plane. The period

of the forked coupling-field is  $d = \lambda_c/2(\sin \theta) \approx 75 \mu\text{m}$ , and its diameter is  $\approx 700 \mu\text{m}$  as measured in the equivalent center of the vapor cell. Similarly, another separated identical Gaussian coupling beam from a beam splitter (BS1),  $E_c^y$ , forms a forked coupling-field in the  $y$ - $z$  plane after experiencing the standing-wave (SW<sub>y</sub>) configuration (see the green box in Figure 1a). All these beams recombine at a beam splitter (BS6) and propagate toward the vapor cell along the  $z$ -direction, driving the transition  $|2\rangle \rightarrow |3\rangle$  with frequency detuning  $\Delta_c = \omega_c - \omega_{23}$ , where  $\omega_{ij}(i, j = 1, 2, 3)$  is the resonant frequency between the states  $|i\rangle$  and  $|j\rangle$ . The 10 cm long atomic vapor cell, wrapped with  $\mu$ -metal sheets, is heated by an oven to provide an atomic density of  $\approx 8.78 \times 10^{12} \text{ cm}^{-3}$  at  $106^\circ\text{C}$ .

A weak probe beam with a Gaussian profile  $E_p$  (with wavelength  $\lambda_p = 780 \text{ nm}$ , frequency  $\omega_p$ , wave vector  $k_p$ ), from an external cavity diode laser (DL pro, Toptica) connecting the transition  $|1\rangle \rightarrow |2\rangle$  with detuning  $\Delta_p = \omega_p - \omega_{12}$ , counter-propagates through the coupling-field lattice inside the atomic medium, where the radius of the probe beam is  $\approx 160 \mu\text{m}$  in the center of the vapor cell. Consequently, it experiences a spatially modulated index of refraction during propagation under the EIT condition. A reference beam, introduced from the original probe beam via a beam splitter (BS7), interacts with  $E_p$  at the position of a charge-coupled device (CCD) camera, which is used to monitor the output probe beam.

Figure 1c schematically illustrates the generation of 1D vortex-beam arrays (eliminating part of SW<sub>y</sub> in Figure 1a) in the proposed system. It is believed that a Gaussian probe beam can be diffracted into multiple beams carrying a tunable OAM after interacting with the 1D forked-photonic lattice along the  $x$ -direction. This photonic lattice is established by the interference of Gaussian and vortex coupling beams, which are symmetrically placed with respect to the  $z$ -axis at a small angle  $2\theta \approx 0.6^\circ$ , as shown in Figure 1d. A 2D forked-photonic lattice in the  $x$ - $y$  plane can be achieved by introducing another set of coupling field in the  $y$ -direction as shown in Figure 1e. The spiral phases of the coupling beams along the  $x$ - and  $y$ -directions are denoted as  $e^{im_x\varphi}$  and  $e^{im_y\varphi}$ , respectively.

Under the slowly varying envelope approximation and steady-state regime,<sup>[17]</sup> the propagation of the probe field in the atomic medium is governed by  $\partial E_p/\partial z = (k_p \text{Im}(\chi) + ik_p \text{Re}(\chi))E_p$  with  $k_p = 2\pi/\lambda_p$  and  $\chi$  being the dielectric susceptibility of the atomic medium. For the cascade-type three-level configuration (Figure 1b) and considering the Doppler broadening effect, the spatially modulated susceptibility experienced by the probe beam can be obtained as (see Section S1, Supporting Information)

$$\chi(\nu)d\nu = i \frac{|\mu_{12}|^2}{\hbar\epsilon_0} \times \left[ \gamma_{21} - i\Delta_p - k_p\nu + \frac{\Omega_{\text{SW}}^2/4}{\gamma_{13} - i(\Delta_p + \Delta_c) - i(k_p - k_c)\nu} \right]^{-1} \times \frac{N}{u\sqrt{\pi}} \exp\left(-\frac{\nu^2}{u^2}\right) d\nu \quad (1)$$

where  $\nu$  is the velocity of the atoms,  $u = \sqrt{2k_B T/M}$  (with  $k_B$  the Boltzmann constant,  $T$  the temperature of the vapor, and  $M$  the atomic mass),  $N$  is the atomic density,  $\epsilon_0$  is the dielectric constant

in vacuum,  $\mu_{ij}$  is the transition dipole momentum between levels  $|i\rangle$  and  $|j\rangle$ ,  $\gamma_{ij} = (\Gamma_i + \Gamma_j)/2$  with  $\Gamma_i$  being the natural decay rate of level  $|i\rangle$ , and  $\Omega_{\text{SW}}$  denotes the effective Rabi frequency of the coupling field, which is given by

$$\Omega_{\text{SW}} = 2\Omega_c^2[1 + \cos(k_c x - m\varphi)] \quad (2)$$

for the 1D case and

$$\Omega_{\text{SW}} = 2\Omega_c^2[2 + \cos(k_c x - m_x\varphi) + \cos(k_c y - m_y\varphi)] \quad (3)$$

for the 2D case. Here,  $\Omega_c = \mu_{23}E_{c1}^x/\hbar$ ,  $k_c = k_{c1}^x \sin(\theta)$ , and  $\varphi = \text{angle}(x + iy)$ . Note that we have taken  $E_{c1}^x = E_{c2}^x = E_{c1}^y = E_{c2}^y$  and  $k_{c1}^x = k_{c2}^x = k_{c1}^y = k_{c2}^y$ . The effective susceptibility  $\chi$  is got by integrating Equation (1).

Then, the transmission function of the probe field at  $z = L$  reads

$$T(x, y) = E_p(x, y, 0)T_a T_p, \quad (4)$$

where  $E_p(x, y, 0)$  is the input probe beam profile, and  $T_a = e^{-k_p \text{Im}(\chi)L}$  and  $T_p = e^{ik_p \text{Re}(\chi)L}$  denote the amplitude and phase modulations, respectively. In the far-field regime, the diffraction intensity distribution is expressed as<sup>[34]</sup>

$$I(X, Y) = \frac{\exp(ik_p z)}{i\lambda_p z} \int_{-\infty}^{\infty} \int_{-\infty}^{\infty} T(x, y) \exp[i\frac{k_p}{2z}(X^2 + Y^2)] dx dy \quad (5)$$

where  $(X, Y)$  is the coordinate of the observation plane, and  $(x, y)$  is the coordinate of the photonic lattice. Equation (5) implies that the diffraction pattern of the probe beam  $E_p(x, y, 0)$  is significantly modulated by the forked-photonic lattice in Equations (2) and (3), resulting in intriguing diffraction behaviors.

### 3. Experimental Realization of Vortex-Beam Arrays

To verify our approach, we examine the generation of 1D vortex-beam arrays based on a 1D forked-photonic lattice (Equation (2)) with a Gaussian probe field propagating in the  $z$ -direction. As shown in Figure 2a, we choose the topological charge of the coupling beam  $m = 1$  and numerically simulate the diffraction pattern of the probe beam based on Equation (5). One finds that a discrete diffraction pattern with topological charge  $\ell(n) = nm = 0, \pm 1, \dots$ , where  $n = \dots - 2, -1, 0, 1, 2 \dots$  denotes the  $n$ th-order diffraction with topological charge  $\ell(n)$ . Figure 2b,c displays the corresponding experimental observations of the output intensities and interference fringes of the probe beam, respectively. The zeroth-order diffraction remains a Gaussian profile, whereas the  $\pm$ first-order diffractions turn into vortex beams with  $\ell = \pm 1$ , respectively. Figure 2d-f represents the same content that Figure 2a-c does, excepting that  $m = 2$ . Clearly, in this case, three diffraction orders with  $\ell = -2, 0, 2$  are observed. Note that, here we focus on  $n = -1, 0, 1$  and ignore the higher-order diffractions with lower powers. The experimental results agree with those of the numerical simulations. By the way, the working wavelength here is 780 nm assisted by the coupling field of 776 nm, and more working wavelengths can be achieved by suitable energy levels of the atom.

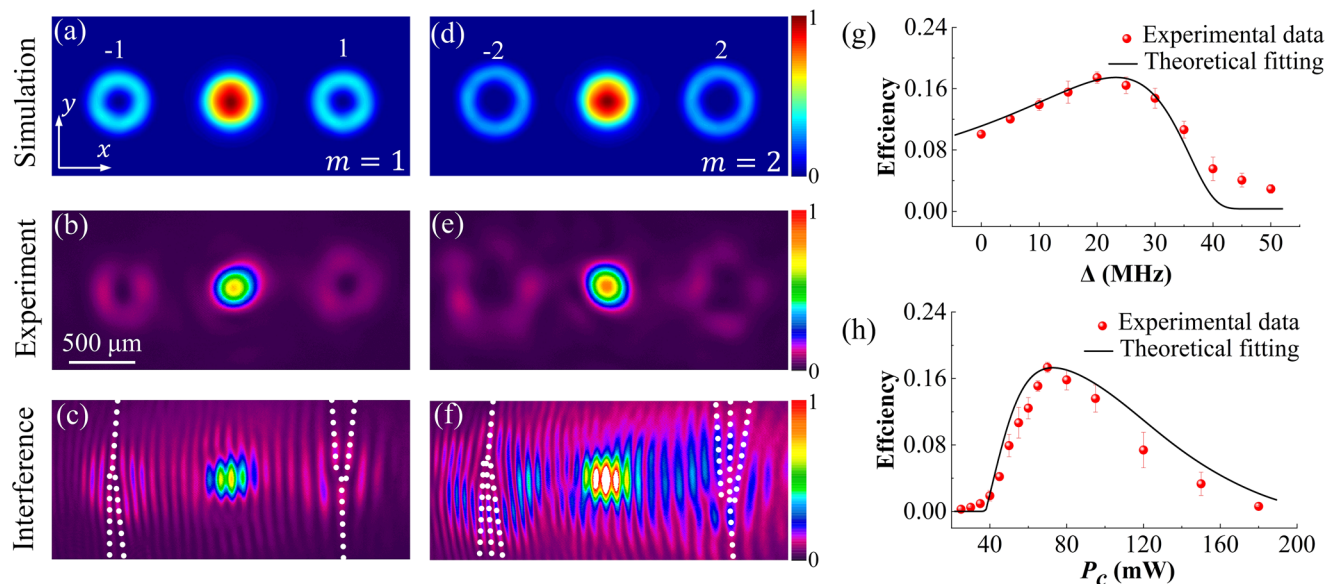


**Figure 2.** a) Numerical simulation (Equation (5)) of the output intensity image of the Gaussian probe beam after traveling through the 1D forked-photonic lattice (Equation (2)) with  $m = 1$ . The other parameters are  $\Delta = \Delta_p + \Delta_c = 2\Gamma_2$ ,  $\Omega_c = 5\Gamma_2$ ,  $\Gamma_1 = 0$ , and  $\Gamma_3 = 0.1\Gamma_2$ . The integers above each diffracted beam denote the topological charge  $\ell$ . b,c) Corresponding experimental observations of the output intensities (b) and interference fringes (c) of the probe Gaussian beam. Here, the two-photon detuning is  $\Delta = 20$  MHz, and the powers of the coupling and probe beams are  $P_c = 70$  and  $P_p = 3.5$  mW, respectively. The power of the probe beam has been made much smaller than that of the coupling beam for ensuring an efficient EIT effect. d–f) The same content as (a–c) but with  $m = 2$ . g) Measured efficiency (red dots) versus  $\Delta$  with  $P_c = 70$  mW. h) Measured efficiency versus  $P_c$  with  $\Delta = 20$  MHz. The black lines represent of the theoretical fitting.

In addition to generating the vortex-beam arrays on-demand by controlling the topological charge  $m$  of the forked-photonic lattices, the intensity of the high-order diffractions (e.g.,  $n = \pm 1$ ) can be enhanced all-optically by various coherence control mechanisms enabled by EIT. To illustrate this, we introduce the diffraction efficiency defined as the ratio of the power measured within a diffractive vortex beam at the output plane to the total outgoing power. Figure 2g presents the measured first-order diffraction efficiency versus two-photon detuning ( $\Delta = \Delta_p + \Delta_c$ ) with  $m = 1$  and coupling field power  $P_c = 70$  mW. As  $\Delta$  increases, the efficiency gradually improves owing to the introduction of both the amplitude and phase modulations when  $\Delta \neq 0$ . By further increasing  $\Delta$  such that the atomic medium becomes more transparent, the efficiency then reduces.<sup>[20]</sup> Figure 2h shows the measured first-order diffraction efficiency versus the power of the coupling beam  $P_c$  at  $\Delta = 20$  MHz. Similarly, an optimal diffraction efficiency occurs at the value of  $P_c = 70$  mW. In the experiment, the maximum diffraction efficiency reaches 18% at  $\Delta = 20$  MHz and  $P_c = 70$  mW. More details are provided in Section S2, Supporting Information.

We shall now discuss the generation of 2D vortex-beam arrays via a 2D forked-photonic lattice (Equation (3)), which is described as the superposition of two perpendicularly oriented (fork) gratings (more details in Section S3, Supporting Information). Here, the topological charge of the  $(n_x, n_y)$ -order diffraction beam is  $\ell(n_x, n_y) = n_x m_x + n_y m_y$  with  $n_{x,y} = 0, \pm 1, \dots$  Figure 3 shows the numerical simulations and corresponding experimental observations of the generated 2D vortex-beam arrays for different  $(m_x, m_y)$ . When all the coupling beams are Gaussian shaped, that is,  $(m_x = 0, m_y = 0)$  (Figure 3a,b), the optically-induced lattice is a standard 2D square lattice. Thus, the Gaus-

sian probe beam is diffracted into a typical square lattice pattern, which remain Gaussian profile. By adding the vortex beam in the  $y$ -direction with  $(m_x = 0, m_y = 1)$  (Figure 3c,d), the  $(n_x, 1)$ -order diffractions become vortex beams with  $\ell(n_x, 1) = 1$ , the  $(n_x, -1)$ -order ones become beams with  $\ell(n_x, -1) = -1$  and the  $(n_x, 0)$ -order ones are still Gaussian shaped. We further investigate the case of  $(m_x = 1, m_y = 1)$ , as shown in Figure 3e,f. It is found that the optical vortex arrays possess inversion symmetry of  $\ell(n_x, n_y) = -\ell(-n_x, -n_y)$  about the central beam.<sup>[8]</sup> The diffraction patterns at  $n_x = -n_y$  are Gaussian beams. The experimental measurements are in agreement with the simulations.

As discussed above, we concentrate on the generation of the vortex-beam arrays of a Gaussian probe beam experiencing forked-photonic lattices. Intriguingly, the topological charges of the vortex-beam arrays can be enriched by a probe beam carrying an OAM. Assuming that the initial input probe beam propagating along the  $z$ -direction is  $E_p(x, y, 0) = \exp(i\ell_p \varphi_p)$  with  $\ell_p$  and  $\varphi_p$  being the topological charge and azimuthal angle,  $\ell'$  of the diffraction pattern depends on the topological charges of both the grating defects and the input beam, that is,  $\ell'(n) = \ell_p + nm$  for the 1D case and  $\ell'(n_x, n_y) = \ell_p + n_x m_x + n_y m_y$  for the 2D case (see Section S4, Supporting Information, for further details). In the experiments, we select  $\ell_p = 1$  for simplicity. Figure 4a–f shows the simulations and measurements of the diffraction patterns of the vortex probe beam traveling through the 1D forked-photonic lattice. The topological charge of the zeroth-order diffraction becomes  $\ell'(0) = 1$  and  $\ell'(\pm 1) = \ell(\pm 1) + 1$  compared with Figure 2. Figure 4g,h shows the simulation and measurement results for the 2D case with  $m_x = 1$  and  $m_y = 1$ , respectively. In contrast to that shown in Figure 3e,f, here, the topological charge of each diffracted beam increases

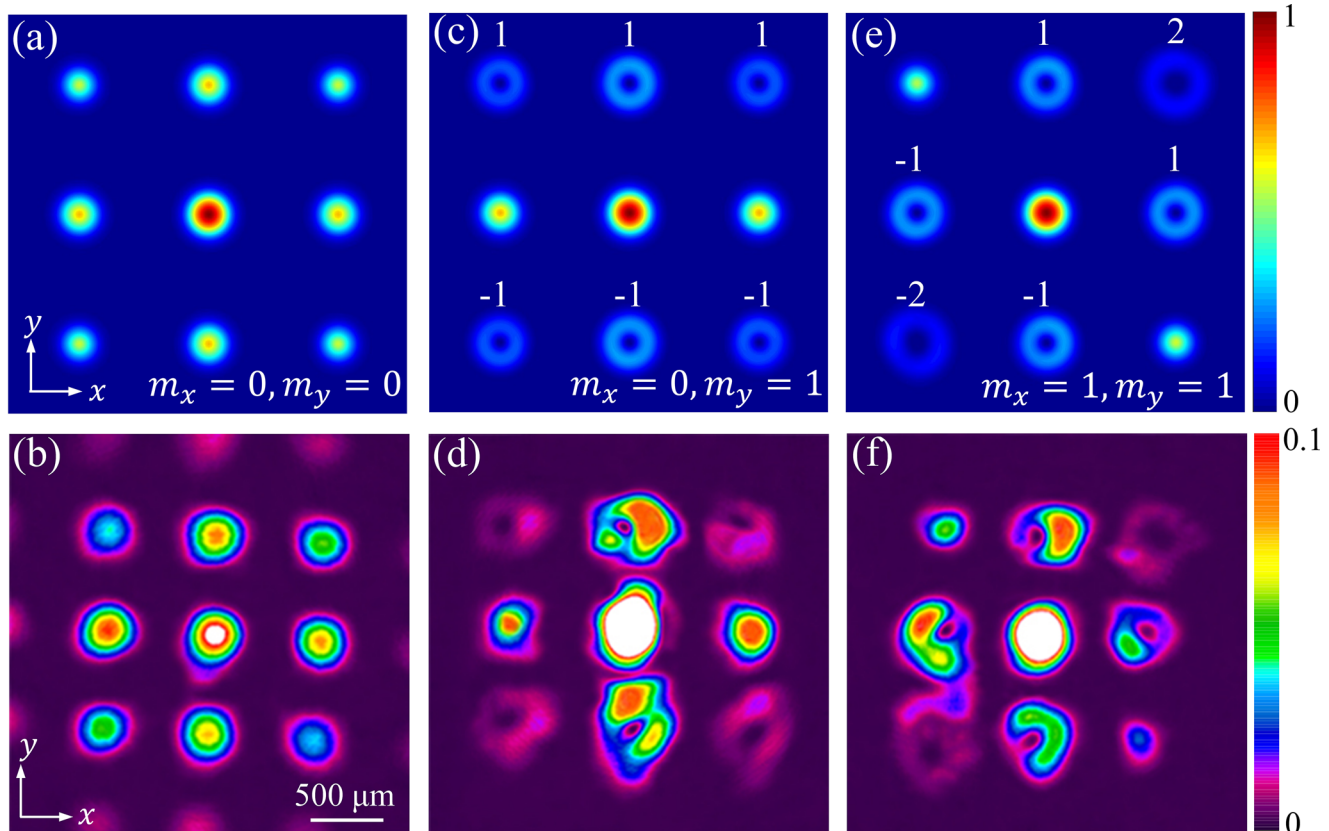


**Figure 3.** a,c,e) Numerical simulations (Equation (5)) of the output intensity image of the Gaussian probe beam after traveling through the 2D forked-photonic lattice (Equation (3)) with  $(m_x = 0, m_y = 0)$  (a),  $(m_x = 0, m_y = 1)$  (c), and  $(m_x = 1, m_y = 1)$  (e). The integers in each subfigure denote the topological charge  $\ell$  of the corresponding diffracted beams. b,d,f) The experimentally observed diffraction patterns corresponding to (a,c,e). Here,  $\Omega_c = 7\Gamma_2$  in simulations, the powers of the coupling and probe beams are  $P_c = 90$  and  $P_p = 6$  mW in experiments, respectively. The other parameters are the same as those in Figure 2.

by  $\ell_p = 1$ , breaking the original inversion symmetry. Remarkably, the efficiencies of all the high-order diffractions are significantly improved with respect to Figure 2 because of the introduction of an additional azimuthal phase  $e^{i\ell_p\phi_p}$  in the phase modulation  $T_p$  of Equation (4)<sup>[35,36]</sup> (see Section S4, Supporting Information).

After confirming the generation of the vortex-beam arrays, the purities of the vortex beams are investigated as well. As an example, we measure the purities of vortex beams generated in Figure 2 (see Section S5, Supporting Information, for more details). The purities of the vortex beams with  $\ell = \pm 1$  are greater than 90%, while those of the beams with  $\ell = \pm 2$  are  $\approx 80\%$ . The purities of higher-order OAM mode beams decrease attributed to the inhomogeneity of the forked-photonic lattices. Such inhomogeneity also leads the imperfections of the experimentally observed patterns especially for 2D cases (Figures 3b,d,f and 4h). In the experiment, the beam divergence and external disturbance in long-distance transmission, as well as the increasing radius of the beam curvature after expansion result in the non-uniformity of the lattices. This can be improved by miniaturizing the experimental system. In fact, vapor cells with a high density at the mm or  $\mu\text{m}$  scale have been extensively researched<sup>[37–39]</sup> and are suitable for the microscale integration of our system.

## 4. Conclusion

In summary, we experimentally demonstrated the generation of 1D and 2D vortex-beam arrays in a coherently prepared cascade-type three-level <sup>85</sup>Rb atomic system. The refractive index experienced by the Gaussian probe is modified by the forked-photonic lattices, which are introduced by the interference of Gaussian and vortex coupling beams. Thus, the atomic medium behaves in the same way that the forked gratings do, enabling the probe beam to be diffracted into vortex-beam arrays with topological charges that can be tuned by the dislocation defects of the forked-photonic lattices. Moreover, the relative efficiency of the high-order ( $\pm$ first) diffraction can be improved by modulating the two-photon detuning and the power of the coupling beams. We also investigated the diffraction of a probe beam with OAM that experience such forked-photonic lattices. The proposed study may pave the way for research on understanding and controlling vortex beams in coherent atomic medium. Moreover, the system is scalable and supports for the generation of large vortex-beam arrays (see Sections S3 and S4, Supporting Information) that can exploit spatial-division multiplexing for optical communications,<sup>[5]</sup> and it is mainly suitable for applications such as optical manipulation and optical machining, which require multidimensional vortex

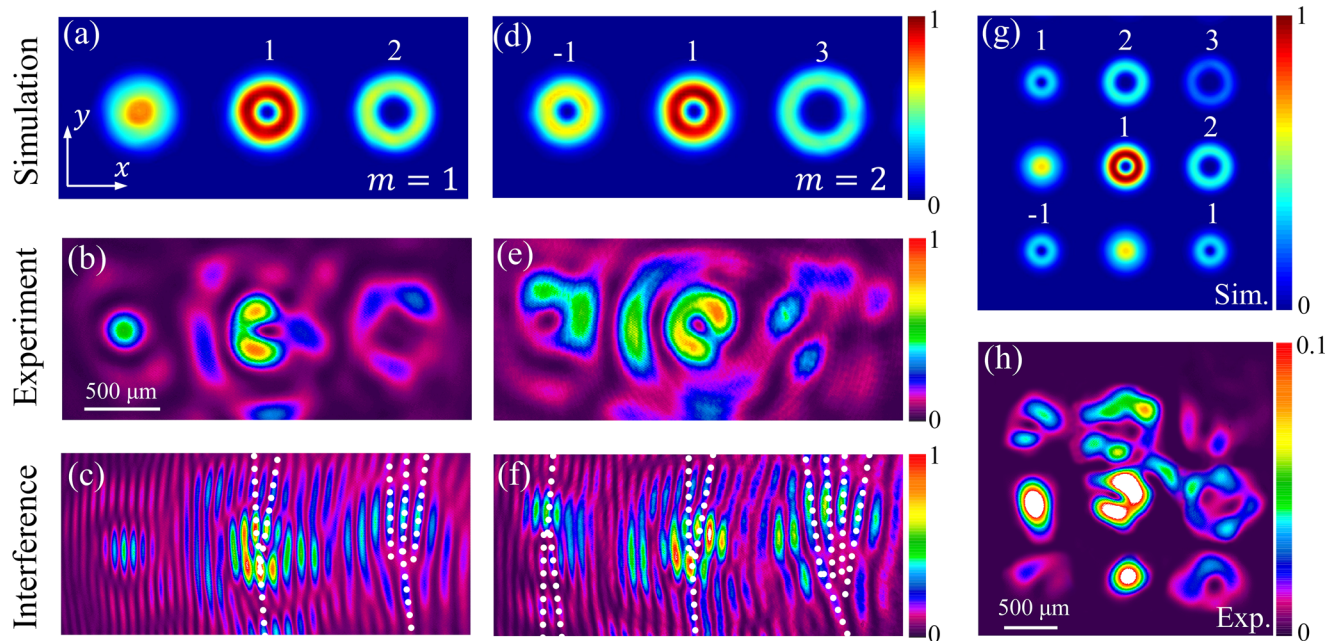


**Figure 4.** a) Numerical simulation (Equation (5)) of the output intensity image of the vortex probe beam after traveling through the 1D forked-photonic lattice (Equation (2)) with  $m = 1$  and  $\ell_p = 1$ . The integers above each diffracted beam denote the topological charge  $\ell'$ . b,c) Experimental observations of the output intensities (b) and interference fringes (c) corresponding to (a). The other parameters are the same as those in Figure 2. d–f) Same as (a–c) but with  $m = 2$ . g,h) Simulation (g) and measurement (h) of the output intensity image of the vortex probe beam after traveling through the 2D forked-photonic lattice (Equation (2)) with  $(m_x = 1, m_y = 1)$  and  $\ell_p = 1$ .

beams with real-time tunable OAMs, intensities, and spatial distribution degrees of freedom.<sup>[40,41]</sup>

Received: September 2, 2022  
Revised: November 19, 2022  
Published online:

## Supporting Information

Supporting Information is available from the Wiley Online Library or from the author.

## Acknowledgements

J.Y. and H.Z. contributed equally to this work. This work was supported by the National Key R&D Program of China (2022YFA1404500, and 2021YFA1400900), the National Natural Science Foundation of China (61875112, 62075121, 12074232, and 12125406), and the fund for Shanxi “1331 Project”.

## Conflict of Interest

The authors declare no conflict of interest.

## Data Availability Statement

The data that support the findings of this study are available from the corresponding author upon reasonable request.

## Keywords

atomic medium, forked-photonic lattices, vortex-beam arrays

- [1] H. He, M. E. J. Friese, N. R. Heckenberg, H. Rubinsztein-Dunlop, *Phys. Rev. Lett.* **1995**, *75*, 826.
- [2] S. Franke-Arnold, L. Allen, M. Padgett, *Laser Photonics Rev.* **2008**, *2*, 299.
- [3] Y. Shen, X. Wang, Z. Xie, C. Min, X. Fu, Q. Liu, M. Gong, X. Yuan, *Light: Sci. Appl.* **2019**, *8*, 90.
- [4] J. Wang, J.-Y. Yang, I. M. Fazal, N. Ahmed, Y. Yan, H. Huang, Y. Ren, Y. Yue, S. Dolinar, M. Tur, A. E. Willner, *Nat. Photonics* **2012**, *6*, 488.
- [5] J. Wang, *Photonics Res.* **2016**, *4*, B14.
- [6] K. Huang, H. Liu, S. Restuccia, M. Q. Mehmood, S.-T. Mei, D. Giovannini, A. Danner, M. J. Padgett, J.-H. Teng, C.-W. Qiu, *Light: Sci. Appl.* **2018**, *7*, 17156.
- [7] P. Chen, B.-Y. Wei, W. Ji, S.-J. Ge, W. Hu, F. Xu, V. Chigrinov, Y.-Q. Lu, *Photon. Res.* **2015**, *3*, 133.
- [8] J. C. T. Lee, S. J. Alexander, S. D. Kevan, S. Roy, B. J. McMorran, *Nat. Photonics* **2019**, *13*, 205.
- [9] T. Lei, M. Zhang, Y. Li, P. Jia, G. N. Liu, X. Xu, Z. Li, C. Min, J. Lin, C. Yu, H. Niu, X. Yuan, *Light: Sci. Appl.* **2015**, *4*, e257.
- [10] L. Chen, J. Lei, J. Romero, *Light: Sci. Appl.* **2014**, *3*, e153.
- [11] L. Xu, C. Wang, X. Qi, R. Li, C. Zhang, L. Zhang, Z. Ren, Z. Zhang, J. Li, Y. Hu, D. Wu, J. Chu, *Appl. Phys. Lett.* **2021**, *119*, 131101.
- [12] Y. Zhuang, S. Wang, Z. Chen, Y. Jia, W. Zhang, Y. Yao, Y. Ren, F. Chen, H. Liu, *Appl. Phys. Lett.* **2022**, *120*, 211101.
- [13] J. Yang, S. Gurung, S. Bej, P. Ni, H. W. H. Lee, *Rep. Prog. Phys.* **2022**, *85*, 036101.

- [14] J. Jin, M. Pu, Y. Wang, X. Li, X. Ma, J. Luo, Z. Zhao, P. Gao, X. Luo, *Adv. Mater. Technol.* **2017**, *2*, 1600201.
- [15] M. Piccardo, M. de Oliveira, A. Toma, V. Aglieri, A. Forbes, A. Ambrosio, *Nat. Photonics* **2022**, *16*, 359.
- [16] H. Sroor, Y.-W. Huang, B. Sephton, D. Naidoo, A. Vallés, V. Ginis, C.-W. Qiu, A. Ambrosio, F. Capasso, A. Forbes, *Nat. Photonics* **2020**, *14*, 498.
- [17] H. Y. Ling, Y.-Q. Li, M. Xiao, *Phys. Rev. A* **1998**, *57*, 1338.
- [18] M. Fleischhauer, A. Imamoglu, J. P. Marangos, *Rev. Mod. Phys.* **2005**, *77*, 633.
- [19] F. Wen, H. Ye, X. Zhang, W. Wang, S. Li, H. Wang, Y. Zhang, C. wei Qiu, *Photon. Res.* **2017**, *5*, 676.
- [20] J. Yuan, C. Wu, L. Wang, G. Chen, S. Jia, *Opt. Lett.* **2019**, *44*, 4123.
- [21] Z. Zhang, J. Feng, X. Liu, J. Sheng, Y. Zhang, Y. Zhang, M. Xiao, *Opt. Lett.* **2018**, *43*, 919.
- [22] Z. Zhang, L. Yang, J. Feng, J. Sheng, Y. Zhang, Y. Zhang, M. Xiao, *Laser Photonics Rev.* **2018**, *12*, 1800155.
- [23] J. Yuan, S. Dong, C. Wu, L. Wang, L. Xiao, S. Jia, *Opt. Express* **2020**, *28*, 23820.
- [24] Y. Zhang, Z. Wang, Z. Nie, C. Li, H. Chen, K. Lu, M. Xiao, *Phys. Rev. Lett.* **2011**, *106*, 093904.
- [25] Z. Zhang, Y. Zhang, J. Sheng, L. Yang, M.-A. Miri, D. N. Christodoulides, B. He, Y. Zhang, M. Xiao, *Phys. Rev. Lett.* **2016**, *117*, 123601.
- [26] Z. Zhang, X. Liu, D. Zhang, J. Sheng, Y. Zhang, Y. Zhang, M. Xiao, *Phys. Rev. A* **2018**, *97*, 013603.
- [27] J. Yuan, C. Wu, Y. Li, L. Wang, Y. Zhang, L. Xiao, S. Jia, *Opt. Express* **2019**, *27*, 92.
- [28] Y. Zhang, D. Zhang, Z. Zhang, C. Li, Y. Zhang, F. Li, M. R. Belić, M. Xiao, *Optica* **2017**, *4*, 571.
- [29] Y. Zhang, Z. Wu, M. R. Belić, H. Zheng, Z. Wang, M. Xiao, Y. Zhang, *Laser Photonics Rev.* **2015**, *9*, 331.
- [30] Y. He, R. Mao, H. Cai, J.-X. Zhang, Y. Li, L. Yuan, S.-Y. Zhu, D.-W. Wang, *Phys. Rev. Lett.* **2021**, *126*, 103601.
- [31] Z. Zhang, R. Wang, Y. Zhang, Y. V. Kartashov, F. Li, H. Zhong, H. Guan, K. Gao, F. Li, Y. Zhang, M. Xiao, *Nat. Commun.* **2020**, *11*, 1902.
- [32] Z. Zhang, S. Liang, F. Li, S. Ning, Y. Li, G. Malpuech, Y. Zhang, M. Xiao, D. Solnyshkov, *Optica* **2020**, *7*, 455.
- [33] S. C. McEldowney, D. M. Shemo, R. A. Chipman, P. K. Smith, *Opt. Lett.* **2008**, *33*, 134.
- [34] J. W. Goodman, *Introduction to Fourier Optics*, Roberts and Company, Greenwood Village, CO **2004**.
- [35] H. R. Hamed, V. Kudriašov, J. Ruseckas, G. Juzeliūnas, *Opt. Express* **2018**, *26*, 28249.
- [36] S. H. Asadpour, H. R. Hamed, T. Kirova, E. Paspalakis, *Phys. Rev. A* **2022**, *105*, 043709.
- [37] J. Keaveney, A. Sargsyan, U. Krohn, I. G. Hughes, D. Sarkisyan, C. S. Adams, *Phys. Rev. Lett.* **2012**, *108*, 173601.
- [38] A. Sargsyan, G. Hakhumyan, A. Papoyan, D. Sarkisyan, A. Atvars, M. Auzinsh, *Appl. Phys. Lett.* **2008**, *93*, 021119.
- [39] A. Sargsyan, A. Amiryan, Y. Pashayan-Leroy, C. Leroy, A. Papoyan, D. Sarkisyan, *Opt. Lett.* **2019**, *44*, 5533.
- [40] C. Zhang, Y. Hanchang, C. Wang, J. Zhang, L. Zhao, H. Zhang, W. Zhu, H. Zhai, W. Dong, K. Sugioka, *Opt. Lett.* **2021**, *46*, 5308.
- [41] K. Toyoda, K. Miyamoto, N. Aoki, R. Morita, T. Omatsu, *Nano Lett.* **2012**, *12*, 3645.